JCARME
ISSN: 2228-7922

Journal of Computational and Applied Research in Mechanical Engineering
Vol. 5, No. 2, pp. 147-160, Spring-Summer 2016
http://jcarme.srttu.edu

Incompressible laminar flow computations by an upwind least-squares meshless method

M. Y. Hashemi[a,*]

[a] *Department of Mechanical Engineering, Azarbaijan Shahid Madani University, Tabriz, 53751-71379, Iran*

Article info:

Received: 07/01/2015
Accepted: 16/08/2015
Online: 03/03/2016

Keywords:
Incompressible laminar artificial compressibility, Least-squares meshless method, Characteristic based scheme.

Abstract

In this paper, the laminar incompressible flow equations are solved by an upwind least-squares meshless method. Due to the difficulties in generating quality meshes, particularly in complex geometries, a meshless method is increasingly used as a new numerical tool. The meshless methods only use clouds of nodes to influence the domain of every node. Thus, they do not require the nodes to be connected to form a mesh and decrease the difficulty of meshing, particularly around complex geometries. In the literature, it has been shown that the generation of points in a domain by the advancing front technique is an order of magnitude faster than the unstructured mesh for a 3D configuration. The Navier–Stokes solver is based on the artificial compressibility approach and the numerical methodology is based on the higher-order characteristic-based (CB) discretization. The main objective of this research is to use the CB scheme in order to prevent instabilities. Using this inherent upwind technique for estimating convection variables at the mid-point, no artificial viscosity is required at high Reynolds number. The Taylor least-squares method was used for the calculation of spatial derivatives with normalized Gaussian weight functions. An explicit four-stage Runge-Kutta scheme with modified coefficients was used for the discretized equations. To accelerate convergence, local time stepping was used in any explicit iteration for steady state test cases and the residual smoothing techniques were used to converge acceleration. The capabilities of the developed 2D incompressible Navier-Stokes code with the proposed meshless method were demonstrated by flow computations in a lid-driven cavity at four Reynolds numbers. The obtained results using the new proposed scheme indicated a good agreement with the standard benchmark solutions in the literature. It was found that using the third order accuracy for the proposed method could be more efficient than its second order accuracy discretization in terms of computational time.

1. Introduction

The governing fluid flow equations are nonlinear partial differential equations, which are solved by numerical methods. Various finite difference methods (FDM) [1, 2], finite volume methods (FVM) [3, 4], and finite elements methods (FEM) [5, 6] have been developed for

*Corresponding author
Email address: m.y.hashemi@azaruniv.ac.ir

incompressible fluid flow in computational fluid dynamics (CFD). The main problem of CFD for incompressible flow is the generation of quality mesh around complex geometries, because low speed of gases and fluid flows are in conflict with complex geometries such as air-condition systems [7, 8], heat-exchanger [9, 10], electronic equipment cooling [11], ocean freight [12], etc.

In general, numerical mesh generation methods are classified as structured and unstructured methods, each of which has its own advantages and disadvantages [13, 14]. Due to the difficulties in generating quality meshes, particularly in complex geometries, a meshless method is increasingly used as a new numerical tool. The meshless methods only use clouds of nodes to influence the domain of every node. Thus, they do not require the nodes to be connected to form a mesh and decrease the difficulty of meshing, particularly around complex geometries. Lohner has shown that the generation of points in domain by the advancing front technique is an order of magnitude faster than that of an unstructured mesh for a 3D configuration [15, 16]. Meshless methods have advantages in terms of moving boundary and large deformations over mesh-based algorithms, in which the spatial domain is discretized using a set of points, as opposed to the cells of a finite volume grid. Clouds are then used to solve the governing equations.

Its applications are to solve any partial differential equations, especially compressible and incompressible fluid flow equations, as well as inviscid and low Reynolds number laminar flows to high Reynolds number turbulent flows.

In a meshless method, the flow derivatives are calculated using different approximation methods, like smooth particle hydrodynamics (SPH) [17], generalized finite difference method (GFDM) [18, 19], element-free Galerkin method (EFGM) [20-22], radial basis function method (RBFM) [23, 24], reproducing kernel particle method (RKPM) [25], meshless local Petrov-Galerkin approach (MLPG) [26, 27], etc.

Meshless method does not involve remeshing process and could easily realize adaptivity strategy. Lohner et al. used finite point method (FPM) for compressible flow solution [28]. Recently, Ortega et al. developed finite point method for solving compressible flow problems involving moving boundaries and adaptivity [29, 30]. The least-squares meshfree method (LSMFM) was used by Hashemi and Jahangirian for compressible viscous and inviscid flow calculations [31, 32] and the convergence behavior and approximation accuracy on Stokes problem by LSMFM were presented [33]. An upwind least-squares based meshless method was analyzed and used by Su et al. for high Reynolds number flow calculations [34].

Many different schemes have been proposed for compressible and incompressible flow solutions by finite difference and finite volume methods. The method of solving low-speed or incompressible flows by artificial compressibility (AC) correction was first introduced by Chorin [35] for obtaining steady state solutions. In this method, a time derivative of the pressure is added to the continuity equation and a coupling system of equations for pressure and velocity is obtained.

By reviewing the literature, it is found that different schemes for the discretization of AC equations have been used in FDM and FVM (for instance, see [3, 36-45]), one of which is the characteristic-based scheme (CB) as an upwind scheme.

Various upwind schemes are used in meshless discretization for compressible flow solution such as Lohner et al. [28], Sridar and Balakrishnan [46], and Praveen and Deshpande [47]. In this work, an explicit meshless solver for incompressible fluid flow was developed. To achieve the discretized form of equations, the Taylor series least-squares method was used for the approximation of derivatives at each node, which led to a central difference spatial discretization. The main objective of this research is to use the CB scheme in order to prevent instabilities. The CB meshless method was applied for two-dimensional lid-driven cavity flow for a wide range of Reynolds numbers and compared with the standard benchmark solutions in the literature in order to show its accuracy and ability.

2. E Governing equations

Incompressible viscous flow can be mathematically described by continuity equation and momentum equations, namely Navier-Stokes (N-S) equations. The conservative variables and non-dimensional form of the N-S equations for two-dimensional incompressible flows modified by the AC correction can be expressed as:

$$\frac{\partial \mathbf{W}}{\partial t}+\frac{\partial \mathbf{F}}{\partial x}+\frac{\partial \mathbf{G}}{\partial y}=\frac{1}{\mathrm{Re}}\left(\frac{\partial \mathbf{R}}{\partial x}+\frac{\partial \mathbf{S}}{\partial y}\right), \qquad (1)$$

where:

$$\mathbf{W}=\begin{bmatrix} p \\ u \\ v \end{bmatrix},\ \mathbf{F}=\begin{bmatrix} \beta u \\ u^2+p \\ u v \end{bmatrix},\ \mathbf{G}=\begin{bmatrix} \beta v \\ u v \\ v^2+p \end{bmatrix},$$
$$\mathbf{R}=\begin{bmatrix} 0 \\ \frac{\partial u}{\partial x} \\ \frac{\partial v}{\partial x} \end{bmatrix},\ \mathbf{S}=\begin{bmatrix} 0 \\ \frac{\partial u}{\partial y} \\ \frac{\partial v}{\partial y} \end{bmatrix},\ \mathrm{Re}=\frac{\rho U_{ref}\mathrm{L}_{ref}}{\mu}. \qquad (2)$$

Here, **W** is the vector of primitive variables, **F, G** and **R, S** are convective and viscous flux vectors, respectively. The artificial compressibility parameter and Reynolds number are shown by β and Re, respectively. In the definition of Reynolds number, L_{ref} is reference length, U_{ref} is reference velocity, and μ and ρ are viscosity and density of fluid, respectively, which are constant in flow field.

3. Discretization of equations

The least-squares meshless method is used to discretize the flow equations in the conservation form. The spatial derivatives of the function using the least-squares method are as follows [48]:

$$\left(\frac{\partial \phi}{\partial x}\right)_i=2\sum_{j=1}^{m}a_{ij}\left(\phi_{j+\frac{1}{2}}-\phi_i\right),$$
$$\left(\frac{\partial \phi}{\partial y}\right)_i=2\sum_{j=1}^{m}b_{ij}\left(\phi_{j+\frac{1}{2}}-\phi_i\right), \qquad (3)$$

where $j+\frac{1}{2}$ is the mid-point of the edge ij, where j is in a cloud of point i and m is the number of neighbors of point i in its cloud (Fig. 1). In the present work, clouds were simply defined as the connectivity of an existing unstructured mesh generated by advancing front algorithm. Minimum and maximum numbers of neighbors were 5 and 7, respectively, and the majority of points had 6 neighbors. The coefficients in Eq. (3) can be calculated using the weighting function as:

$$a_{ij}=\frac{\omega_{ij}\Delta x_{ij}\sum_{k=1}^{m}\omega_{ik}\Delta y_{ik}^2-\omega_{ij}\Delta y_{ij}\sum_{k=1}^{m}\omega_{ik}\Delta x_{ik}\Delta y_{ik}}{\left(\sum_{k=1}^{m}\omega_{ik}\Delta x_{ik}^2\right)\left(\sum_{k=1}^{m}\omega_{ik}\Delta y_{ik}^2\right)-\left(\sum_{k=1}^{m}\omega_{ik}\Delta x_{ik}\Delta y_{ik}\right)^2}, \qquad (4)$$
$$b_{ij}=\frac{\omega_{ij}\Delta y_{ij}\sum_{k=1}^{m}\omega_{ik}\Delta y_{ik}^2-\omega_{ij}\Delta x_{ij}\sum_{k=1}^{m}\omega_{ik}\Delta x_{ik}\Delta y_{ik}}{\left(\sum_{k=1}^{m}\omega_{ik}\Delta x_{ik}^2\right)\left(\sum_{k=1}^{m}\omega_{ik}\Delta y_{ik}^2\right)-\left(\sum_{k=1}^{m}\omega_{ik}\Delta x_{ik}\Delta y_{ik}\right)^2},$$

where ω is an arbitrary weighting function such as normalized Gaussian (Fig. 2),

$$\omega_{ij}=\frac{e^{-\left(\frac{|\vec{r}_{ij}|}{c}\right)^2}}{1-e^{-\left(\frac{|\vec{r}_{ij}|}{d}\right)^2}},\ \left|\vec{r}_{ij}\right|=\sqrt{\Delta x_{ij}^2+\Delta y_{ij}^2}, \qquad (5)$$
$$r_d=\left(1+\varepsilon_g\right)r_{\max},\ c=\mathrm{K}r_d$$

where $r_{\max}$ is the maximum value of $\left|\vec{r}_{ij}\right|$ for point i. In practice, $\varepsilon_g=1$ and $\mathrm{K}=0.5$ provide the most accurate results [49].

By applying the least-squares approximations given by Eq. (3) to each component of flux functions in Eq. (1), a semi-discrete form of the N-S equations at point i is obtained:

$$\frac{\partial \mathbf{W}_i}{\partial t}+2\left[\sum_{j=1}^{m}a_{ij}\left(\mathbf{F}_{j+\frac{1}{2}}-\mathbf{F}_i\right)+\sum_{j=1}^{m}b_{ij}\left(\mathbf{G}_{j+\frac{1}{2}}-\mathbf{G}_i\right)\right]=\mathrm{RHS} \qquad (6)$$
$$\mathrm{RHS}=\frac{2}{\mathrm{Re}}\left[\sum_{j=1}^{m}a_{ij}\left(\mathbf{R}_{j+\frac{1}{2}}-\mathbf{R}_i\right)+\sum_{j=1}^{m}b_{ij}\left(\mathbf{S}_{j+\frac{1}{2}}-\mathbf{S}_i\right)\right]$$

If the arithmetic averaging of primitive variables and their derivations is used at the mid-point to calculate the convective and viscous fluxes, the flow equations discretization

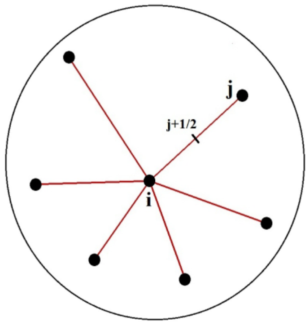

Fig. 1. Scheme of the point and its neighbors.

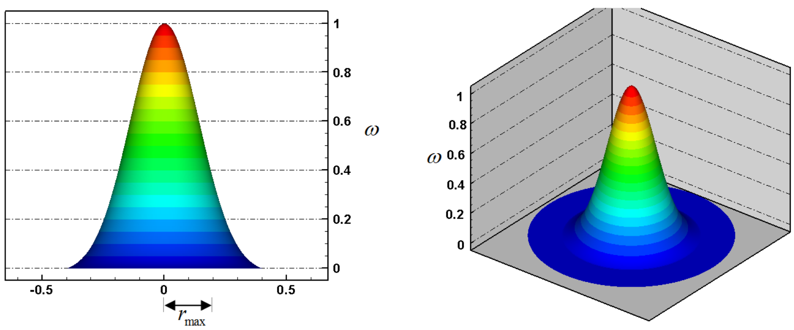

(a) (b)

Fig. 2. Visual representation of the normalized Gaussian weight function ($\varepsilon_g = 1$, and $K = 0.5$).

could lead to checkerboard pattern and the above equation represents unstable discretization. Therefore, it is necessary to modify the variables and their gradients at the mid-points to remove solution instability. For carrying out the checkerboard pattern in viscous flux, the derivation of any variable Φ is calculated as follows[50, 51]:

$$\nabla\Phi_{j+\frac{1}{2}} = \overline{\nabla\Phi}_{j+\frac{1}{2}} - \left[\overline{\nabla\Phi}_{j+\frac{1}{2}} \bullet \vec{s}_{ij} - \frac{\Phi_j - \Phi_i}{|\vec{r}_{ij}|}\right]\vec{s}_{ij} \quad , \qquad (7)$$

$$\vec{r}_{ij} = \Delta x_{ij}\vec{i} + \Delta y_{ij}\vec{j}$$

where $\vec{s}_{ij}$ is the unit vector between i and j or $\left(\frac{\vec{r}_{ij}}{|\vec{r}_{ij}|}\right)$ and $\overline{\nabla\Phi}_{j+\frac{1}{2}}$ is the average of the gradient at mid-point $\left(\frac{\nabla\Phi_i + \nabla\Phi_j}{2}\right)$. $\nabla\Phi_i$ is evaluated using the least-squares method of Eq. (3) as follows;

$$\nabla\Phi_i = \left[\sum_{j=1}^{m} a_{ij}\left(\Phi_j - \Phi_i\right)\right]\vec{i} + \left[\sum_{j=1}^{m} b_{ij}\left(\Phi_j - \Phi_i\right)\right]\vec{j} \qquad (8)$$

For example, to calculate $\frac{\partial u}{\partial y}$ and $\frac{\partial v}{\partial x}$ at the mid-point:

$$\left(\frac{\partial u}{\partial y}\right)_{j+\frac{1}{2}} = \overline{\left(\frac{\partial u}{\partial y}\right)}_{j+\frac{1}{2}} - \left[\overline{\left(\frac{\partial u}{\partial x}\right)}_{j+\frac{1}{2}}\Delta x_{ij} + \overline{\left(\frac{\partial u}{\partial y}\right)}_{j+\frac{1}{2}}\Delta y_{ij} - u_j - u_i\right]\frac{\Delta y_{ij}}{\vec{r}_{ij}\bullet\vec{r}_{ij}} \quad , \qquad (9)$$

$$\left(\frac{\partial v}{\partial x}\right)_{j+\frac{1}{2}} = \overline{\left(\frac{\partial v}{\partial x}\right)}_{j+\frac{1}{2}} - \left[\overline{\left(\frac{\partial v}{\partial x}\right)}_{j+\frac{1}{2}}\Delta x_{ij} + \overline{\left(\frac{\partial v}{\partial y}\right)}_{j+\frac{1}{2}}\Delta y_{ij} - v_j - v_i\right]\frac{\Delta x_{ij}}{\vec{r}_{ij}\bullet\vec{r}_{ij}}$$

Viscous terms of the Navier-Stokes equations can produce the dissipative property necessary to stabilize the numerical scheme. It can be shown that the discretization procedure is stable if the local Reynolds number for any cloud point is less than two [52]. This limitation leads to the high number of points in flow domain and low computational efficiency. Thus, artificial dissipation terms or upwind schemes have to be used to stabilize the equations. In this work, the CB as the upwind scheme was used for the first time to stabilize the equations. The CB meshless method is explained in the following sections.

4. Conventional characteristic-based meshless method

The conventional CB scheme interpolation was used in this paper for comparison with the new proposed method. In this section, CB scheme relations which were used here to calculate the primitive variables were presented. It should be noted that these relations were based on the CB scheme presented in the works such as [53-55], in which derivation of relations have been completely explained. If $\left(s_x, s_y\right)$ denotes the unit vector in edge ij direction (Fig. 1), the relations for determining flow quantities at the mid-point $\left(j+\frac{1}{2}\right)$ are as follows:

$$
\begin{aligned}
&u_{j+\frac{1}{2}} = fs_x + u^o s_y^2 - v^o s_x s_y, \\
&v_{j+\frac{1}{2}} = fs_y + v^o s_x^2 - u^o s_x s_y, \\
&p_{j+\frac{1}{2}} = p^1 - \lambda_1\left[\left(u_{j+\frac{1}{2}} - u^1\right)s_x + \left(v_{j+\frac{1}{2}} - v^1\right)s_y\right]
\end{aligned}
\tag{10}
$$

where:

$$
\begin{aligned}
&f = \frac{1}{2\sqrt{\left(\lambda^0\right)^2+\beta}}\left[\left(p^1-p^2\right)+\left(\lambda^1 u^1-\lambda^2 u^2\right)s_x + \left(\lambda^1 v^1 - \lambda^2 v^2\right)s_y\right] \\
&\lambda^0 = \bar{u}_{j+\frac{1}{2}} s_x + \bar{v}_{j+\frac{1}{2}} s_y \ , \\
&\lambda^1 = \lambda^0 + \sqrt{\left(\lambda^0\right)^2+\beta} \ , \\
&\lambda^2 = \lambda^0 - \sqrt{\left(\lambda^0\right)^2+\beta} \ , \\
&\bar{u}_{j+\frac{1}{2}} = \frac{1}{2}\left(u_i+u_j\right), \ \bar{v}_{j+\frac{1}{2}} = \frac{1}{2}\left(v_i+v_j\right)
\end{aligned}
\tag{11}
$$

Flow quantities at a new time level obtained from the above equations on the locally one-dimensional characteristics were used to calculate fluxes at the mid-point. The quantities at the prior time level were evaluated by upwind method using the sign of characteristics as follows:

$$
\mathbf{W}^k = \frac{1}{2}\left[\left(1+\operatorname{sign}\left(\lambda^k\right)\right)\mathbf{W}_L + \left(1-\operatorname{sign}\left(\lambda^k\right)\right)\mathbf{W}_R\right] \tag{12}
$$

where $\mathbf{W}$ is the vector containing the characteristic values for each k =0, 1, 2 and the values of $\mathbf{W}_L$ and $\mathbf{W}_R$ are obtained by the high-order upwind-biased interpolation which is similar to the approach presented in [56].

$$
\begin{aligned}
&\mathbf{W}_L = \mathbf{W}_i + \frac{1}{4}\left[\left(1-\kappa\right)\Delta_i^- + \left(1+\kappa\right)\Delta_i^+\right], \\
&\mathbf{W}_R = \mathbf{W}_j - \frac{1}{4}\left[\left(1-\kappa\right)\Delta_j^+ + \left(1+\kappa\right)\Delta_j^-\right],
\end{aligned}
\tag{13}
$$

where:

$$
\begin{aligned}
&\Delta_i^+ = \Delta_j^- = \mathbf{W}_j - \mathbf{W}_i \ , \\
&\Delta_i^- = 2\vec{r}_{ij} \bullet \nabla\mathbf{W}_i - \left(\mathbf{W}_j - \mathbf{W}_i\right), \\
&\Delta_j^+ = 2\vec{r}_{ij} \bullet \nabla\mathbf{W}_j - \left(\mathbf{W}_j - \mathbf{W}_i\right).
\end{aligned}
\tag{14}
$$

Therefore,

$$
\begin{aligned}
&\mathbf{W}_L = \mathbf{W}_i + \frac{1}{2}\left[\left(1-\kappa\right)\vec{r}_{ij} \bullet \nabla\mathbf{W}_i + \kappa\Delta_i^+\right], \\
&\mathbf{W}_R = \mathbf{W}_j - \frac{1}{2}\left[\left(1-\kappa\right)\vec{r}_{ij} \bullet \nabla\mathbf{W}_j + \kappa\Delta_j^-\right],
\end{aligned}
\tag{15}
$$

where κ is set to 0 and $\frac{1}{3}$, which corresponds to a nominally second and third order accuracy, respectively. The gradients of $\mathbf{W}$ at i and j are calculated by least-squares coefficients.

5. Time discretization

An explicit fourth order Runge-Kutta scheme with modified coefficients was used for the time discretizaion of spatially discretized equations as follows [32]:

$$
\begin{aligned}
&\frac{\partial \mathbf{W}_i}{\partial t}+\mathbf{Q}_i\left(\mathbf{W}\right)=0,\\
&\mathbf{W}_i^{(1)}=\mathbf{W}_i^{(n)}-\alpha_1\Delta t_i\mathbf{Q}_i\left(\mathbf{W}^{(n)}\right),\\
&\mathbf{W}_i^{(2)}=\mathbf{W}_i^{(n)}-\alpha_2\Delta t_i\mathbf{Q}_i\left(\mathbf{W}^{(1)}\right),\\
&\mathbf{W}_i^{(3)}=\mathbf{W}_i^{(n)}-\alpha_3\Delta t_i\mathbf{Q}_i\left(\mathbf{W}^{(2)}\right),\\
&\mathbf{W}_i^{(4)}=\mathbf{W}_i^{(n)}-\alpha_4\Delta t_i\mathbf{Q}_i\left(\mathbf{W}^{(3)}\right),\\
&\mathbf{W}_i^{(n+1)}=\mathbf{W}_i^{(4)}\\
&\alpha_1=0.333\ ,\ \alpha_2=0.267\ ,\\
&\alpha_3=0.500,\ \alpha_4=1.000
\end{aligned}
\tag{16}
$$

where $\mathbf{Q}$ contains the convective and viscous fluxes. The maximum time step was determined by:

$$
\begin{aligned}
&\Delta t_i=\frac{\mathrm{CFL}}{\sum_{j=1}^{m}\left(\left|\bar{u}_{j+\frac{1}{2}}a_{ij}+\bar{v}_{j+\frac{1}{2}}b_{ij}\right|+\bar{c}\sqrt{a_{ij}^2+b_{ij}^2}\right)}\ ,\\
&\bar{c}=\sqrt{\left(\vec{V}_{j+\frac{1}{2}}\bullet\vec{s}_{ij}\right)^2+\beta}\ ,\\
&\vec{V}_{j+\frac{1}{2}}=\bar{u}_{j+\frac{1}{2}}\vec{i}+\bar{v}_{j+\frac{1}{2}}\vec{j}\ ,\ \vec{V}_{j+\frac{1}{2}}=\frac{1}{2}\left(\vec{V}_i+\vec{V}_j\right)
\end{aligned}
\tag{17}
$$

To accelerate convergence, local time stepping was used in any explicit iteration for steady state test cases [33]. In addition, the original residuals ($\mathbf{Q}$) might be replaced with the smoothed residuals $\tilde{\mathbf{Q}}$ by solving the implicit equation with two or three Jacobi iterations [57]:

$$
\begin{aligned}
&\tilde{\mathbf{Q}}_i=\mathbf{Q}_i+\varepsilon\Delta^2\tilde{\mathbf{Q}}_i\ ,\\
&\Delta^2\tilde{\mathbf{Q}}_i=\sum_{j=1}^{m}\left(\tilde{\mathbf{Q}}_j-\tilde{\mathbf{Q}}_i\right)=\sum_{j=1}^{m}\tilde{\mathbf{Q}}_j-m\tilde{\mathbf{Q}}_i
\end{aligned}
\tag{18}
$$

At each point i, $\Delta^2\tilde{\mathbf{Q}}_i$ represents the undivided Laplacian of the most recent residuals and ε is the smoothing coefficient, which was chosen equal to 0.5 in this research.

6. Boundary conditions

For viscous flows on a solid boundary, a no-slip boundary condition needs to be imposed. Therefore, for any point on the stationary solid boundary, velocity components are:

$$
u_i=0\ ,\ \ v_i=0\ ,
\tag{19}
$$

and the momentum governing equations on the solid boundary will be:

$$
\begin{aligned}
&\left(\frac{\partial p}{\partial x}\right)_i=\frac{1}{\mathrm{Re}}\left(\frac{\partial^2 u}{\partial x^2}+\frac{\partial^2 u}{\partial y^2}\right)_i\ ,\\
&\left(\frac{\partial p}{\partial y}\right)_i=\frac{1}{\mathrm{Re}}\left(\frac{\partial^2 v}{\partial x^2}+\frac{\partial^2 v}{\partial y^2}\right)_i
\end{aligned}
\tag{20}
$$

Calculation of the viscous terms of Eqs. (20) leads to pressure gradient on the solid boundary. Therefore, pressure gradient on the normal direction to the solid boundary can be evaluated as:

$$
\begin{aligned}
&\left(\frac{\partial p}{\partial n}\right)_i=(\nabla p)_i\bullet\vec{n}_i\ \ ,\left(\frac{\partial p}{\partial n}\right)_i=\sum_{j=1}^{m}\alpha_{ij}\left(p_j-p_i\right),\\
&\nabla=\frac{\partial}{\partial x}\vec{i}+\frac{\partial}{\partial y}\vec{j}\ \ ,\ \ \alpha_{ij}=\left(a_{ij},b_{ij}\right)\bullet\vec{n}_i\ ,
\end{aligned}
\tag{21}
$$

where $\vec{n}_i$ is the unit normal vector to solid boundary at point i and α_{ij} is the component of least-squares coefficient vector in $\vec{n}_i$ direction. Therefore,

$$
\begin{aligned}
&(\nabla p)_i\bullet\vec{n}_i=\sum_{j=1}^{m}\alpha_{ij}\left(p_j-p_i\right),\\
&\Rightarrow\ p_i=\frac{\sum_{j=1}^{m}\alpha_{ij}p_j-(\nabla p)_i\bullet\vec{n}_i}{\sum_{j=1}^{m}\alpha_{ij}},
\end{aligned}
\tag{22}
$$

The upwind least-squares meshless algorithm can be summarized as follows:

STEP1: Start

STEP2: Read the data structure and calculate the least-squares coefficients (Eq. (4)).

STEP3: Make an initial guess for p, u, and v.

STEP4: Calculate the flow parameters at pseudo time level and the mid-point $\left(u_{j+\frac{1}{2}}, v_{j+\frac{1}{2}}, p_{j+\frac{1}{2}}\right)$ by Eq. (10) using flow properties at points i and j at the previous time level.

STEP5: Evaluate the flow parameters at the boundary points (Eqs. (19) and (22)).

STEP6: Calculate the space derivatives of the governing equation for any points in domain (Eq. (6)).

STEP7: Use the explicit fourth order Runge–Kutta scheme to modify the flow parameters (Eq. (16)).

STEP8: Investigate the convergence trends; if yes, go to **STEP9**; else, go to **STEP4**.

STEP9: Export the outputs.

STEP10: Stop

7. Results and discussion

To compare the accuracy and verify the ability of the proposed meshless method, lid-driven cavity flow at four Reynolds numbers were calculated in this paper. All the computations were carried out on a Pentium PC Dual core with 2.00 GHz speed. The AC parameter (β) was equal to 1 in all the cases. The CFL number equaled 1.5 for all the cases. For investigating the convergence trends, the continuity residual was computed as the following definition;

$$\text{Error} = \frac{\sum_{i=1}^{N} \frac{\left|p_i^{n+1} - p_i^n\right|}{\Delta t_i}}{N} \tag{23}$$

where N is the number of points in the domain.

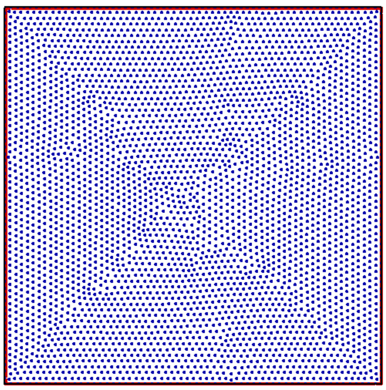

Fig. 3. Point distribution inside the cavity with 60 points on each wall (used for Re=100).

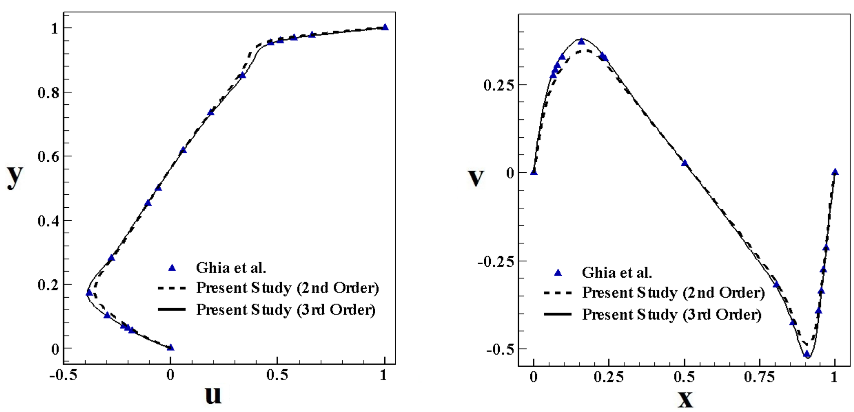

Fig. 4. Comparing the predicted mid-plane velocity profiles for u and v at Re = 1000.

Incompressible steady state flow equations were solved for the cavity flow at the Reynolds numbers of 100, 400, 1000, and 3200 (based on moving wall velocity and cavity length). The sample point's distribution is shown in Fig. 3, which included 4031 points in the domain and 60 points on the cavity's walls and used for solving Reynolds number 100. There were 71, 91, and 121 points on each wall and there were 5646, 9282, and 16401 points inside the domain for Re=400, 1000, and 3200, respectively.
First, the solution of steady flow at Re=1000 was presented. Results obtained for u-velocity profile along vertical line and v-velocity profile along the horizontal line passing through the center of the cavity using the second and third upwind least-squares meshless methods are presented in Fig. 4 in comparison with Ghia et al.'s [58] results. As demonstrated in Fig. 4, the third order accuracy provided more accurate results than the second order accuracy on the same point distribution. Convergence histories of the second and third order accuracies are shown in Fig. 5 which demonstrated better convergence rate of the second order over the third one using the same point distributions. Computational times for any of the iterations of the second and third order accuracies were equal, because only a value of κ varied in Eq. (13).
A point distribution study was performed in this case for the second order accuracy to be compared with the efficiency of the third order accuracy in computational cost. Three computational point distributions including 9282, 12615, and 16401 points were regarded as coarse, medium, and fine point distributions, respectively. There were 105 points on each wall for the medium point distribution.
The velocity profiles along horizontal and vertical lines passing through the center of the cavity for three different point distributions are demonstrated in Fig. 6. It is evident from this figure that the coarse distribution results were not so accurate. However, no significant difference could be recognized between the medium and fine point distribution results, as obtained accuracies for the second order scheme with 12615 points and the third order scheme with 9282 points were the same.
The convergence history is shown in Fig. 7, which could demonstrate the efficiency of the third order accuracy over the second order accuracy.
Results obtained for u-velocity profile along vertical line and v-velocity profile along horizontal line passing through the center of the cavity using characteristic-based upwind least-squares meshless method with the third order accuracy are presented in Figs. 8-10 for different Reynolds numbers. As shown, the obtained results were in good agreement with Ghia et al.'s [58] benchmark solution that was shown by delta symbols in the figures. Figure 11 shows the computed streamlines of the flow field on the contours of velocity magnitude for different Reynolds.

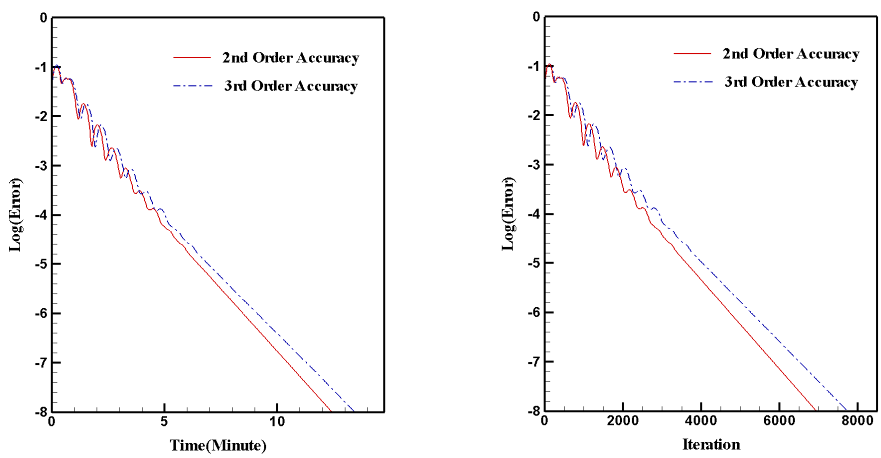

Fig. 5. Convergence history of the second and third order accuracy discretization for the same point distributions at Re=1000.

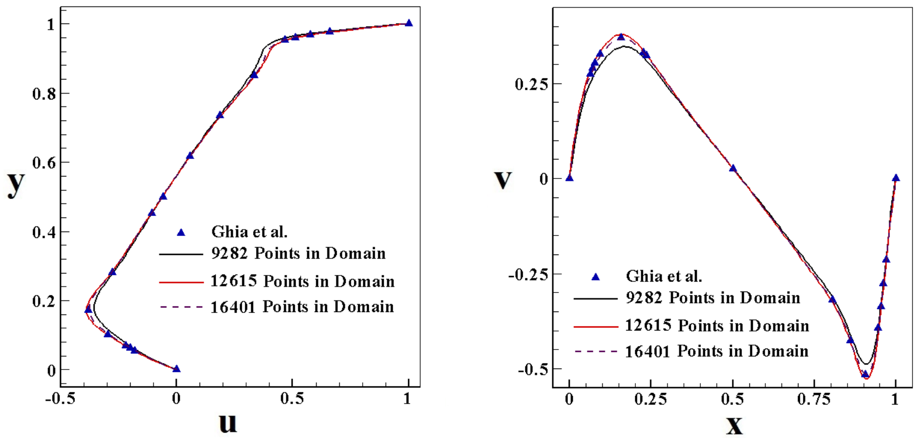

Fig. 6. Computed velocity profiles along the horizontal and vertical lines passing through the cavity center at three point distributions at Re=1000.

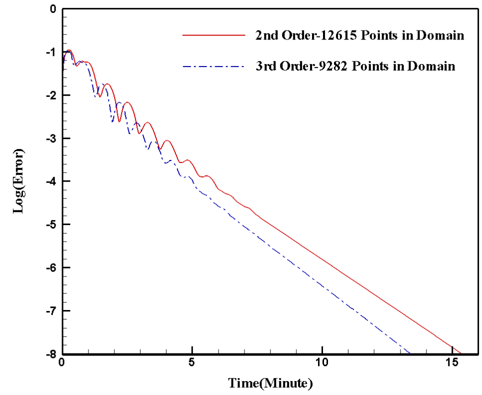

Fig. 7. Convergence history of the second and third order accuracy discretization with the same velocity profiles along horizontal and vertical lines passing through the center of the cavity compared with Ghia's [58] results.

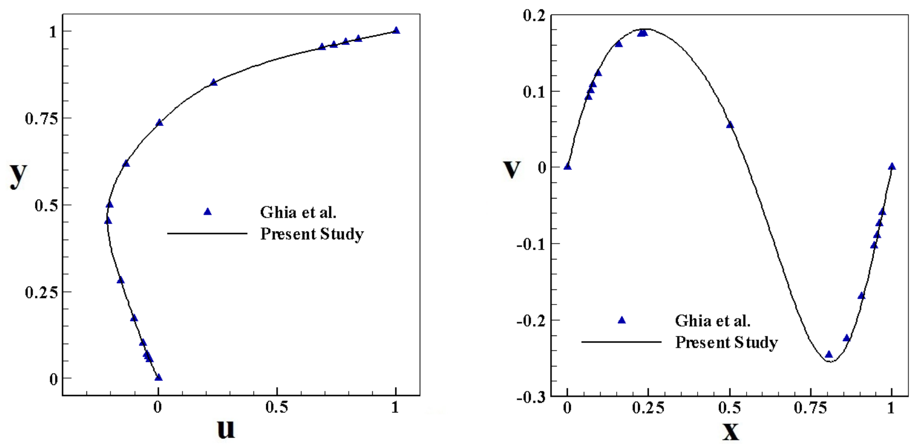

Fig. 8. Comparing the predicted mid-plane velocity profiles for u and v at Re = 100.

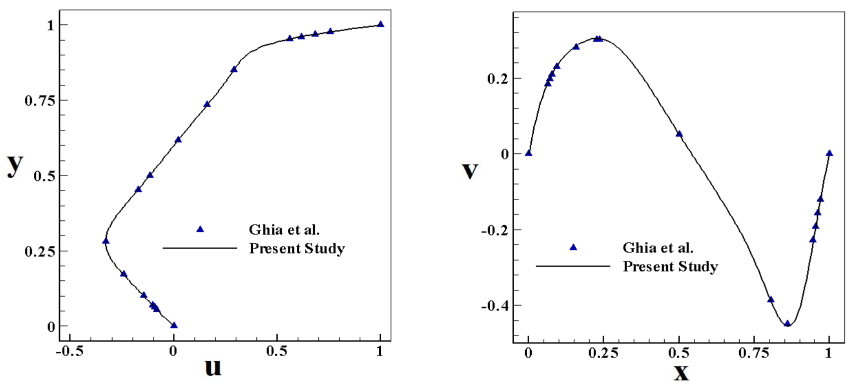

Fig. 9. Comparing the predicted mid-plane velocity profiles for u and v at Re = 400.

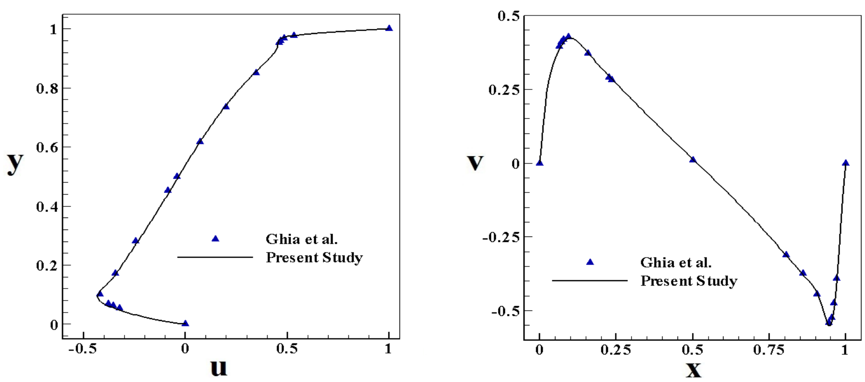

Fig. 10. Comparing the predicted mid-plane velocity profiles for u and v at Re = 3200.

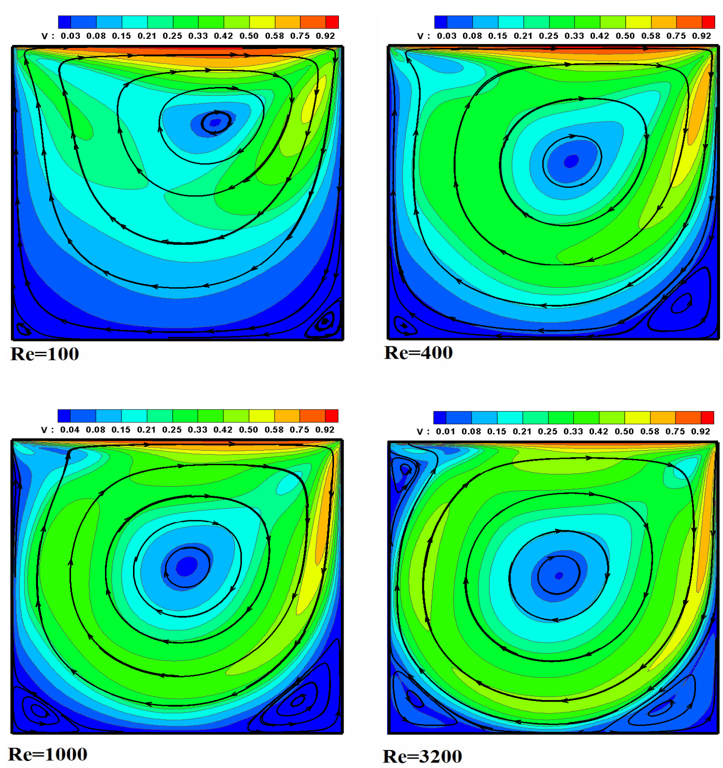

Fig. 11. Streamlines and velocity magnitude contours of the flow field for different Reynolds numbers.

8. Conclusions

In this study, an upwind least-squares meshless method which prevented the instabilities of the central difference spatial discretization was proposed to solve the incompressible laminar flow equations modified by the artificial compressibility. The proposed method was used to solve steady incompressible-driven cavity flow in a wide range of Reynolds numbers. The computed results were in good agreement with the available benchmark solutions in the literature. It was found that using the third order accuracy for the proposed method was more efficient than its second order accuracy discretization in terms of computational time.

References

[1] Y. Morinishi, T. S. Lund, O. V. Vasilyev and P. Moin, "Fully conservative higher order finite difference schemes for incompressible flow", *Journal of Computational Physics*, Vol. 143, pp. 90-124, (1998).

[2] T. Ikeno and T. Kajishima, "Finite-difference immersed boundary method consistent with wall conditions for incompressible turbulent flow simulations", *Journal of Computational Physics*, Vol. 226, No. 2, pp. 1485-1508, (2007).

[3] S. E. Razavi, K. Zamzamian and A. Farzadi, "Genuinely multidimensional characteristic-based scheme for incompressible flows", *International Journal for Numerical Methods in Fluids*, Vol. 57, No. 8, pp. 929-949, (2008).

[4] M. Y. Hashemi and A. Jahangirian, "Simulation of high-speed flows by an unstructured grid implicit method including real gas effects", *International Journal for Numerical Methods in Fluids*, Vol. 56, No. 8, pp. 1281-1287, (2007).

[5] X. Wang and X. Li, "Numerical simulation of three dimensional non Newtonian free surface flows in injection molding using ALE finite element method", *Finite Elements in Analysis and Design*, Vol. 46, No. 7, pp. 551-562, (2010).

[6] R. W. Lewis, K. Ravindran and A. S. Usmani, "Finite element solution of incompressible flows using an explicit segregated approach", *Archives of Computational Methods in Engineering*, Vol. 2, No. 4, pp. 69-93, (1999).

[7] J. H. Kent, "Air Conditioning Modelling by Computational Fluid Dynamics", *Architectural Science Review*, Vol. 37, No. 3, pp. 103-113, (1994).

[8] S. Wang and D. Zhub, "Application of CFD in retrofitting air-conditioning systems in industrial buildings", *Energy and Buildings*, Vol. 35, No. 9, pp. 893-902, (2003).

[9] S. W. Hwang, D. H. Kim, J. K. Min and J. H. Jeong, "CFD analysis of fin tube heat exchanger with a pair of delta winglet vortex generators", *Journal of Mechanical Science and Technology*, Vol. 26, No. 9, pp. 2949-2958, (2012).

[10] M. Yataghene and J. Legrand, "A 3D-CFD model thermal analysis within as craped surface heat exchanger", *Computers & Fluids*, Vol. 71, pp. 380-399, (2013).

[11] S. Aradag, U. Olgun, F. Aktrk and B. Basibyk, "CFD analysis of cooling of electronic equipment as an undergraduate design project", *International Journal of Hydrogen Energy*, Vol. 20, No. 1, pp. 103-113, (2012).

[12] H. Sadat-Hosseini H, Pablo Carrica, F. Stern, N. Umeda, H. Hashimoto, S. Yamamura and A. Mastuda,"CFD, system-based and EFD study of ship dynamic instability events: Surf-riding, periodic motion, and broaching", *Ocean Engineering*, Vol. 38, No. 1, pp. 88-110, (2011).

[13] J. F. Thompson, F. C. Thomas and C. W. Mastin, "Automated numerical generation of body fitted curvilinear co-ordinate system for field containing any number of arbitrary 2D bodies", *Journal of Computational Physics*, Vol. 15, pp. 299-319, (1974).

[14] N. P. Weatherill, "A method for generating irregular computational grids in multiply connected planar domains",

International Journal for Numerical Methods in Fluids, Vol. 8, pp. 181-197, (1998).

[15] R. Lohner and E. Onate, "An advancing front point generation technique", *Communications in Numerical Methods in Engineering*, Vol. 14, No. 12, pp. 1097-1108, (1998).

[16] R. Lohner and E. Onate, "A general advancing front technique for filling space with arbitrary objects", *International Journal for Numerical Methods in Engineering*, Vol. 61, No. 12, pp. 1977-1991, (2004).

[17] P. W. Randles and L. D. Libersky, "Smoothed particle hydrodynamics: some recent improvements and applications", *Computer Methods in Applied Mechanics and Engineering*, Vol. 139, No. 1, pp. 375- 408, (1996).

[18] C. S. Chew CS, K. S. Yeo and C. Shu,"A generalized finite-difference (GFD) ALE scheme for incompressible flows around moving solid bodies on hybrid meshfree-Cartesian grids", *Journal of Computational Physics*, Vol. 218, No. 2, pp. 510-548, (2006).

[19] H. Ding, C. Shu, K. S. Yeo and D. Xu, "Development of least-square-based two-dimensional finite-difference schemes and their application to simulate natural convection in a cavity", *Computers & Fluids*, Vol. 33, No. 1, pp. 137-154, (2004).

[20] S. N. Atluri and T. Zhu, "A new meshless local Petrov-Galerkin (MLPG) approach", *Computational Mechanics*, Vol. 22, No. 2, pp. 117-127, (1998).

[21] J. S. Chen, C. T. Wux, S. Yoon and Y. You, "A stabilized conforming nodal integration for Galerkin mesh-free methods", *International Journal for Numerical Methods in Engineering*, Vol. 50, No. 2, pp. 435-466, (2001).

[22] M. Polner, L. Pesch and J. J. W. van der Vegt, "Construction of stabilization operators for Galerkin least-squares discretizations of compressible and incompressible flows", *Computer Methods in Applied Mechanics and Engineering*, Vol. 196, pp. 2431-2448, (2007).

[23] C. Shu, and B. E. Richards, "Application of generalized differential quadrature to solve two-dimensional incompressible Navier-Stokes equations", *International Journal for Numerical Methods in Fluids*, Vol. 15, No. 7, pp. 791-798, (1992).

[24] H. Q. Chen and C. Shu, "An efficient implicit mesh-free method to solve two dimensional compressible Euler equations", *International Journal of Modern Physics*, Vol. 16, No.3, pp. 439-454, (2005).

[25] W. K. Liu, S. Jun and Y. F. Zhang, "Reproducing kernel particle methods", *International Journal for Numerical Methods in Fluids*, Vol. 20, No. 8-9, pp. 1081-1106, (1995).

[26] M. Najafi, A. Arefmanesh, and V. Enjilela, "Meshless local Petrov-Galerkin method-higher Reynolds numbers fluid flow applications", *Engineering Analysis with Boundary Elements*, Vol. 36, No. 11, pp. 1671-1685, (2012).

[27] Y. L. Wu, G. R. Liu and Y. T. Gu, "Application of meshless local Petrov-Galerkin (MLPG) approach to simulation of incompressible flow", *Numerical Heat Transfer*, Vol. 48, No. 5, pp. 459-475, (2005).

[28] R. Lohner, C. Sacco, E. Onate and S. Idelsohn, "A finite point method for compressible flow", *International Journal for Numerical Methods in Engineering*, Vol. 53, pp. 1765-1779, (2002).

[29] E. Ortega, E. Onate, S. Idelsohn and R. Flores, "A meshless finite point method for three-dimensional analysis of compressible flow problems involving moving boundaries and adaptivity", *International Journal for Numerical Methods in Fluids*, Vol. 73, No. 4, pp. 323-343, (2013).

[30] Z. Ma, H. Chen and C. Zhou, "A study of point moving adaptivity in gridless method", *Computer Methods in Applied Mechanics and Engineering*, Vol. 197, pp. 926-1937, (2008).

[31] Y. Hashemi, and A. Jahangirian, "Implicit fully mesh-less method for compressible viscous flow calculations", *Journal of Computational and Applied Mathematics*, Vol. 235, No. 16, pp. 4687-4700, (2011).

[32] M. Y. Hashemi, and A. Jahangirian,"An efficient implicit mesh-less method for compressible flow calculations", *International Journal for Numerical Methods in Fluids*, Vol. 67, No. 6, pp. 754-770, (2011).

[33] X. K. Zhang, K. C. Kwon and S. K. Youn, "The least-squares meshfree method for the steady incompressible viscous flow", *Journal of Computational Physics*, Vol. 206, pp. 182-207, (2005).

[34] X. Su, S.Yamamoto and K. Nakahashi, "Analysis of a meshless solver for high Reynolds number flow", *International Journal for Numerical Methods in Fluids*, Vol. 72, No. 5, pp. 505-527, (2013).

[35] A. J. Chorin, "A numerical method for solving incompressible viscous flow problems", *Journal of Computational Physics*, Vol. 2, No. 1, pp. 12-26, (1967).

[36] J. Farmer, L. Martinelli and A. Jameson, "Fast multigrid method for solving incompressible hydrodynamic problems with free surface", *American Institute of Aeronautics and Astronautics Journal*, Vol. 32, pp. 1175-1182, (1994).

[37] V. Esfahanian and P. Akbarzadeh, "The Jameson's numerical method for solving the incompressible viscous and in viscid flows by means of artificial compressibility and preconditioning method", *Applied Mathematics and Computation*, Vol. 206, pp. 651-661, (2008).

[38] C. Liu, X. Zheng and C. H. Sung, "Preconditioned multigrid methods for unsteady incompressible flows", *Journal of Computational Physics*, Vol. 139, No. 1, pp. 35-57, (1998).

[39] Y. Kallinderis and H. T. Ahn, "Incompressible Navier-Stokes method with general hybrid meshes", *Journal of Computational Physics*, Vol. 210, No. 1, pp. 75-108, (2005).

[40] D. Drikakis, P. A. Govatsos and D. E. Papantonis, "A characteristic based method for incompressible flows", *International Journal for Numerical Methods in Fluids*, Vol. 19, No. 8, pp. 667-685, (1994).

[41] D. Drikakis, O. P. Iliev and D. P. Vassileva, "A nonlinear multigrid method for the three-dimensional incompressible Navier-Stokes equations", *Journal of Computational Physics*, Vol. 146, No. 1, pp. 301-321, (1998).

[42] K. Siong and C. Y. Zhao, "Numerical study of steady/unsteady flow and heat transfer in porous media using a characteristics-based matrix-free implicit FV method on unstructured grids", *International Journal of Heat and Fluid Flow*, Vol. 25, pp. 1015-1033, (2004).

[43] E. Shapiro and D. Drikakis, "Artificial compressibility, characteristics-based schemes for variable density, incompressible, multi-species flows. Part I. Derivation of different formulations and constant density limit", *Journal of Computational Physics*, Vol. 210, No. 2, pp. 584-607, (2005).

[44] E. Shapiro and D. Drikakis, "Artificial compressibility, characteristics-based schemes for variable density, incompressible, multi-species flows. Part II. Multi grid implementation and numerical tests", *Journal of Computational Physics*, Vol. 210, pp. 608-631, (2005).

[45] M. Y. Hashemi and K. Zamzamian,"A multidimensional characteristic-based method for making incompressible flow calculations on unstructured grids", *Journal of Computational and Applied Mathematics*, Vol. 259(B), pp.795-805, (2014).

[46] S. Sridar and N. Balakrishnan , "An upwind finite difference scheme for meshless solvers", *Journal of Computational Physics*, Vol. 189, No. 1, pp.1-29, (2003).

[47] C. Praveen C. and S. M. Deshpande, "Kinetic meshless method for compressible flows", *International*

Journal for Numerical Methods in Fluids, Vol. 55, No. 11, pp.1059-1089, (2007).

[48] H. Luo, J. D. Baum and R. Lohner, "Hybrid building-block and gridless method for compressible flows", *International Journal for Numerical Methods in Fluids*, Vol. 59, No. 4, pp. 459-474, (2009).

[49] A. Katz, "*Meshless methods for computational fluid dynamics*", .2009, PhD Thesis, Stanford University, (2009).

[50] A. Katz and A. Jameson, "Meshless scheme based on alignment constraints", *American Institute of Aeronautics and Astronautics Journal*, Vol. 48, No. 11, pp. 2501-2511, (2010).

[51] G. May and Jameson, "Unstructured algorithms for inviscid and viscousflows embedded in a unified solver architecture Flo3xx", *AIAA 43rd Aerospace Sciences Meeting 2005*; 0318, Reno, Nevada, (2005).

[52] C. Hirsch, *Numerical Computation of Internaland External Flows (Volume 1:Fundamentals of Computational FluidDynamics)*, 2nd edition, Elsevier, Burlington, pp. 357-360, (2007).

[53] K. Zamzamian and S. E. Razavi, "Multidimensional up winding for incompressible flows based on characteristics", *Journal of Computational Physics*, Vol. 227, No. 19, pp. 8699-8713, (2008).

[54] Y. Zhao and B. Zhang, "A high-order characteristics upwind FV method for incompressible flow and heat transfer simulation on unstructured grid", *Computer Methods in Applied Mechanics and Engineering*, Vol. 190, No. 5, pp. 733-756, (2000).

[55] C. H. Tai and Y. Zhao, "Parallel unsteady incompressible viscous flow computations using an unstructured multigrid method", *Journal of Computational Physics*, Vol. 192, No. 1, pp. 277-311, (2003).

[56] R. Lohner, C. Sacco, E. Onate, S. A. Idelsohn,"Finite point method for compressible flow", *International Journal for Numerical Methods in Engineering,* Vol. 53, pp.1765–1779, (2002).

[57] D. J. Mavriplis, A. Jameson, and L. Martinelli,"Multigrid solution of the Navier-Stokes equations on the triangular meshes", AIAA paper, *27th Sciences Meeting*, Reno, Nevada, USA, January 9-12, (1989).

[58] U. Ghia, K. N. Ghia, and C. T. Shin, "High-Re solutions for incompressible flow using the Navier-Stokes equations and a multigrid method", *Journal of Computational Physics*, Vol. 48, pp.387-411, (1982).